Excitatory selective LTP of supramammillary glutamatergic/GABAergic cotransmission potentiates dentate granule cell firing

Eri Tabuchi[a], Takeshi Sakaba[a], and Yuki Hashimotodani[a,1] (iD)

Emerging evidence indicates that the functionally opposing neurotransmitters, glutamate and GABA, are coreleased from the same presynaptic terminals in some adult brain regions. The supramammillary nucleus (SuM) is one region that coreleases glutamate and GABA in the dentate gyrus (DG) through its afferents. Although the SuM-DG pathway has been implicated in various brain functions, little is known about the functional roles of the peculiar features of glutamate/GABA corelease. Here, we show that depolarization of granule cells (GCs) triggers postsynaptic long-term potentiation (LTP) of glutamatergic, but not GABAergic, cotransmission at SuM-GC synapses. Moreover, the burst activity of perforant-path inputs heterosynaptically induces LTP at excitatory SuM-GC synapses. This non-Hebbian LTP requires postsynaptic Ca^{2+} influx, Ca^{2+}/calmodulin-dependent protein kinase II (CaMKII) activity, and exocytosis of AMPA receptors. Glutamatergic transmission-selective expression of LTP increases the excitatory drive such that SuM inputs become sufficient to discharge GCs. Our results highlight a form of LTP, which dynamically and rapidly changes the glutamatergic/GABAergic cotransmission balance and contributes to DG network activity.

corelease | supramammillary nucleus | dentate gyrus | LTP | depolarization

The dentate gyrus (DG) is the first stage within the hippocampal formation to receive entorhinal cortical inputs and send excitatory outputs to the CA3 region (1), and plays an important role in memory formation, particularly pattern separation, a process of transforming similar patterns of cortical information to nonoverlapping patterns of CA3 outputs (2, 3). Through this process, the DG contributes to the encoding and discrimination of memories (4). The DG also receives subcortical inputs from several brain regions, and these inputs modulate DG functions (1, 3, 4). The supramammillary nucleus (SuM) of the hypothalamus is one subcortical region that projects to the DG and CA2 region (5, 6). With direct connections and indirect connections via the medial septum to the hippocampus, SuM activity is involved in the hippocampal θ rhythm (7, 8). Recent studies have indicated that the SuM projection to the DG is related to spatial memory retrieval (9), sleep and arousal (10–12), and contextual novelty (13). Despite emerging evidence that the SuM-DG pathway contributes to several brain functions, it remains unknown how the SuM afferents to the DG are involved in brain functions at the cellular, synaptic and circuit levels.

Recent studies have revealed that the SuM neurons make monosynaptic connections to granule cells (GCs), the DG principal neurons, and corelease glutamate and GABA onto GCs (10, 12–15). This glutamatergic and GABAergic cotransmission exerts a net excitatory effect on GCs and modulates GC firing through temporal association with entorhinal cortical inputs (14, 15). Similar corelease of glutamate and GABA from the same presynaptic terminals in the mature brain has been reported in the lateral habenula from the entopeduncular nucleus (16–19) and the ventral tegmental area inputs (18, 20, 21), in the ventral tegmental area from the ventral pallidum inputs (21), and in the CA1 pyramidal cells from subsets of hippocampal interneurons (INs) (22, 23). In single axon terminals, glutamate and GABA are cotransmitted from distinct synaptic vesicles in the lateral habenula and presumably in the DG (18). This peculiar form of synaptic transmission, corelease of neurotransmitters with opposing effects (excitation and inhibition), has led to speculation about several possible synaptic functions, including excitation/inhibition balance, gain control, filtering, and regulation of synaptic plasticity (24–26). Intriguingly, the corelease of glutamate and GABA demonstrates plasticity. In the lateral habenula, GABAergic cotransmission was reduced in animal models of depression (16) or in the mice of cocaine withdrawal (19). These changes arise from presynaptic modifications, such as impairment of vesicular GABA filling following the reduction of glutamic acid decarboxylase (GAD) or vesicular GABA

Significance

It is now established that many neurons can release multiple transmitters. Recent studies revealed that fast-acting neurotransmitters, glutamate and GABA, are coreleased from the same presynaptic terminals in some adult brain regions. The dentate gyrus (DG) granule cells (GCs) are innervated by the hypothalamic supramammillary nucleus (SuM) afferents that corelease glutamate and GABA. However, how these functionally opposing neurotransmitters contribute to DG information processing remains unclear. We show that glutamatergic, but not GABAergic, cotransmission exhibits long-term potentiation (LTP) at SuM-GC synapses. By the excitatory selective LTP, the excitation/inhibition balance of SuM inputs increases, and GC firing is enhanced. This study provides evidence that glutamatergic/GABAergic cotransmission balance is rapidly changed in an activity-dependent manner, and such plasticity may modulate DG activity.

Author affiliations: [a]Graduate School of Brain Science, Doshisha University, Kyoto 610-0394, Japan

transporter (VGAT). Additionally, in the hippocampal INs, disruption of GABA synthesis by inhibition of GAD or feeding mice a vitamin B6-deficient diet, a manipulation that decreases GAD activity, reduced GABAergic cotransmission with enhanced glutamatergic cotransmission, indicating the homeostatic control of the glutamate/GABA corelease ratio (22). Thus, the imbalances in glutamatergic and GABAergic cotransmission are associated with neurological disorders and homeostatic scaling. While these alterations are induced over long time scales (16, 19, 22), it is unknown whether activity-dependent rapid changes in glutamatergic and GABAergic cotransmission are induced under physiological conditions, and if so, whether such plasticity can modulate overall neural activity in the circuits.

In this study, we examined whether activity-dependent long-term plasticity is induced at SuM-GC synapses and contributes to DG information processing. We found that repetitive depolarizing pulses or burst firing of GCs induced glutamatergic cotransmission-selective long-term potentiation (LTP) at SuM-GC synapses. This LTP is expressed postsynaptically and requires Ca^{2+} influx through L-type voltage-dependent Ca^{2+} channels (L-VDCCs), postsynaptic Ca^{2+}/calmodulin-dependent protein kinase II (CaMKII) activity, and exocytosis of AMPA receptors (AMPARs). By selective expression of glutamatergic—but not GABAergic—LTP, glutamatergic transmission plays a dominant role in SuM-GC synaptic transmission and excites GCs to trigger action potentials (APs). Thus, our findings provide evidence that SuM-GC glutamate/GABA corelease synapses undergo rapid and enduring activity-dependent changes in synaptic transmission, and such synaptic plasticity may modulate DG information processing and contribute to SuM-DG circuit-linked brain functions.

Results

Postsynaptic Depolarization Induces LTP at Excitatory SuM-GC Synapses. To investigate whether SuM-GC synapses undergo activity-dependent long-term plasticity, we performed whole-cell patch-clamp recordings from GCs in acute hippocampal slices. To optogenetically activate SuM fibers in the DG, we stereotactically injected a Cre-dependent adeno-associated virus (AAV) to express channelrhodopsin-2 (ChR2) [AAV-DIO-ChR2(H134R)-eYFP] into the SuM of VGluT2-Cre mice (Fig. 1A and *SI Appendix*, Fig. S1) (14). By delivering blue light pulses, we recorded optically evoked excitatory postsynaptic currents (oEPSCs) at SuM-GC synapses in the presence of picrotoxin to block inhibitory currents. We first tested whether excitatory SuM-GC synapses exhibit classic NMDAR-dependent Hebbian LTP. To test this, we applied a pairing protocol (200 light pulses at 2 Hz, paired with 0-mV postsynaptic depolarization), a commonly used protocol to induce Hebbian LTP (27). We found that this pairing protocol induced robust LTP of SuM-GC oEPSCs (Fig. 1B) (control: 217 ± 23% of baseline, $n = 10$, $P < 0.001$, paired t test). Unexpectedly, this LTP was not abolished by the NMDAR blocker D-AP5 (Fig. 1B) (D-AP5: 210 ± 26% of baseline, $n = 8$, $P < 0.001$, paired t test; control vs. D-AP5: $P = 0.81$, unpaired t test). This result suggests that excitatory SuM-GC synapses undergo NMDAR-independent LTP by the pairing protocol. To test whether NMDAR-independent LTP requires associative presynaptic and postsynaptic activity, we delivered solo presynaptic activation or postsynaptic depolarization. To our surprise, postsynaptic depolarization (depol) without presynaptic stimulation still caused LTP (Fig. 1B) (depol: 214 ± 21% of baseline, $n = 9$, $P < 0.001$, paired t test; control vs.

depol: $P = 0.89$, unpaired t test), whereas solo presynaptic stimulation failed to induce LTP (Fig. 1B) (pre only; 100 ± 6% of baseline, $n = 4$, $P > 0.98$, Wilcoxon signed rank test). These results suggest that postsynaptic depolarization only can induce LTP at excitatory SuM-GC synapses.

Several previous studies have demonstrated that postsynaptic depolarization induces LTP at CA3-CA1 synapses of the hippocampus (28–31). To test whether excitatory SuM-GC synapses also undergo similar non-Hebbian plasticity by a much shorter duration of postsynaptic depolarization than the pairing protocol (100 s in Fig. 1B), we applied repeated depolarizing pulses (2-s duration repeated 10 times every 5 s from a holding potential of –60 mV to 0 mV). We found that depolarizations of GCs induced robust LTP of excitatory SuM-GC transmission (depol-eLTP), which peaked within 10 min and maintained stable potentiation for up to 60 min (Fig. 1C) (196 ± 19% of baseline, $n = 13$, $P < 0.001$, paired t test). In subsequent experiments, we used the repeated depolarizing pulses as the standard induction protocol for depol-eLTP. The magnitude of the depol-eLTP depended on the number of depolarizing pulses (Fig. 1D). To test whether depol-eLTP could be induced by physiologically relevant GC activity, we applied burst APs in GCs at the θ frequency, which mimics the in vivo firing pattern of GCs that show sparse activity with intermittent burst firing at θ oscillations (32–34). We found that AP firing in GCs (10 bursts of APs at 5 Hz, repeated five times every 5 s) in current-clamp mode using a more physiological K^+-based intracellular solution induced robust LTP (Fig. 1E) (172 ± 17% of baseline, $n = 8$, $P < 0.01$, paired t test). Consistent with the NMDAR-independence of LTP induced by the pairing protocol (Fig. 1B), depol-eLTP induced by repeated depolarizing pulses was also intact in the presence of D-AP5 (Fig. 1F) (202 ± 27% of baseline, $n = 10$, $P < 0.01$, paired t test), suggesting an NMDAR-independent mechanism for depol-eLTP. These results indicate that excitatory SuM-GC synapses express an NMDAR-independent form of non-Hebbian LTP following postsynaptic depolarization.

Depolarization of GCs Exhibits Postsynaptic LTP of SuM-GC AMPAR-Mediated Transmission but Not GABAergic Cotransmission. We next tested whether depol-eLTP is expressed pre- or postsynaptically. By monitoring the paired-pulse ratio (PPR), a commonly used index of presynaptic change, we found that the PPR was not changed after induction of depol-eLTP of SuM-GC AMPAR-oEPSCs (before: 0.52 ± 0.05; LTP: 0.49 ± 0.03, $n = 10$, $P = 0.49$, Wilcoxon signed rank test) (Fig. 1F). Moreover, depol-eLTP increased the amplitude, but not the frequency, of asynchronous SuM-GC oEPSCs in the presence of strontium (Fig. 2A) (amplitude: before: 9.7 ± 0.24 pA; after: 14.1 ± 0.44 pA, $n = 7$, $P < 0.001$, paired t test; frequency: before: 3.7 ± 0.31 Hz; after: 3.7 ± 0.34 Hz, $n = 7$, $P = 0.92$, paired t test). These results suggest that depol-eLTP is likely expressed postsynaptically. To further test the potential involvement of presynaptic changes during depol-eLTP, we investigated the effects of depolarizing pulses on NMDAR-mediated synaptic transmission at SuM-GC synapses. If depol-eLTP is caused by a long-lasting increase in glutamate release, both AMPAR- and NMDAR-mediated synaptic transmission will be equally potentiated. We found that pharmacologically isolated SuM-GC NMDAR-oEPSCs were detectable at –60 mV, even in the presence of 1.3 mM Mg^{2+} (Fig. 2B and *SI Appendix*, Fig. S2). This observation allows us to deliver the same magnitude of depolarization (from –60 to 0 mV) as AMPAR-oEPSCs for monitoring NMDAR-oEPSCs. Unlike
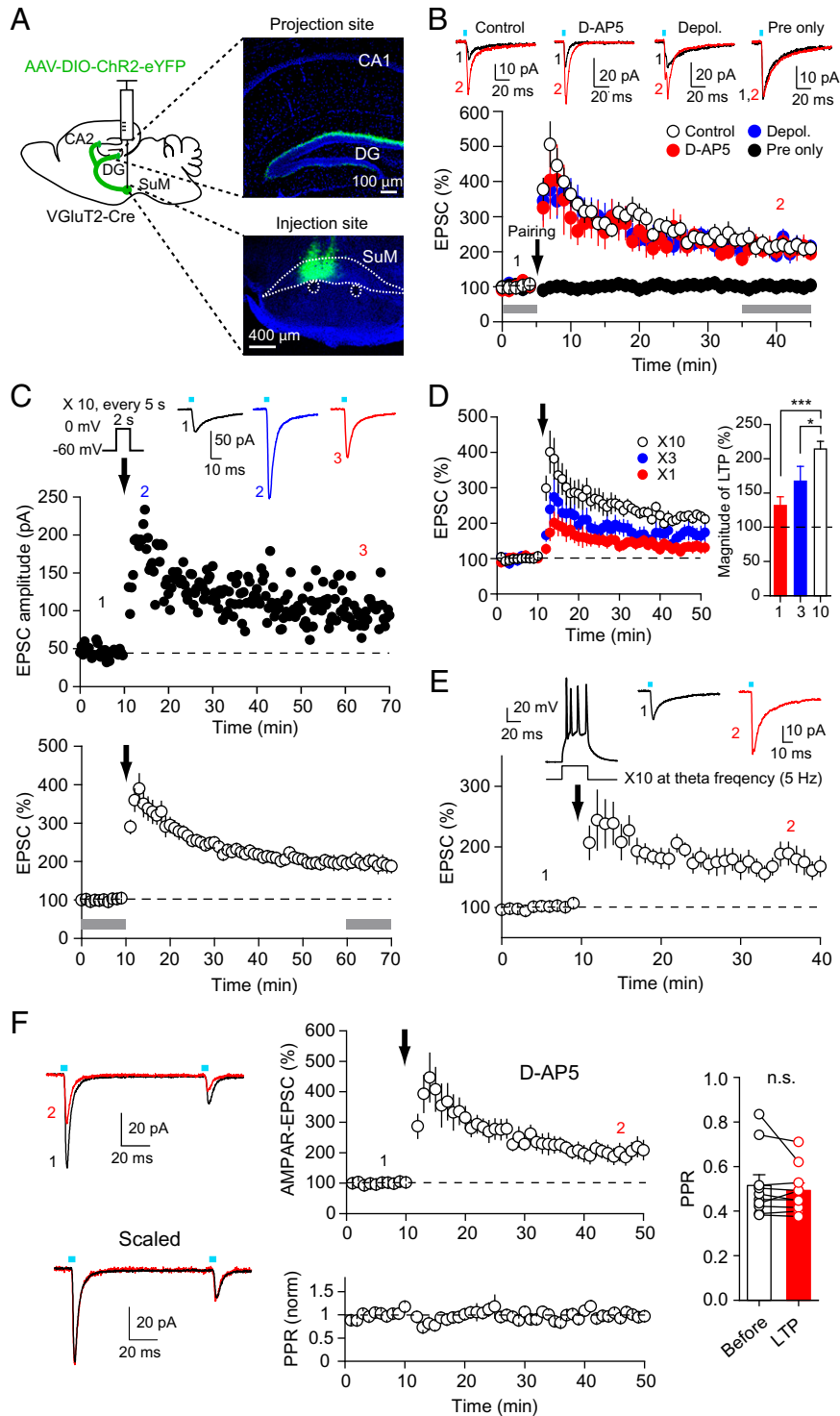
Fig. 1. Depolarization of GCs exhibits LTP of glutamatergic SuM-GC cotransmission. (*A, Left*) Diagram illustrating injection of AAV-DIO-ChR2(H134R)-eYFP into the SuM of VGluT2-Cre mouse. (*Right*) Confocal images showing ChR2(H134R)-eYFP-expressing SuM axons in the DG (*Upper*) and injection site (*Lower*). (*B*) A pairing protocol (200 light pulses at 2 Hz, paired with 0-mV postsynaptic depolarization, arrow) induced robust LTP of SuM-GC oEPSCs (white circle). Same pairing protocol still induced LTP in the presence of 50 μM D-AP5 (red circle). Postsynaptic depolarization without presynaptic activity also induced LTP (blue circle), whereas presynaptic activity without postsynaptic depolarization failed to induce LTP (black circle). Representative traces, which correspond to the numbers in the time-course plot below (for this and all subsequent figures), are shown on the top. For this and all subsequent figures, blue bars indicate the time when blue light was delivered to slices. (*C*) Representative experiment (*Upper*) and summary plot (*Lower*) shows repeated depolarizations (2-s duration repeated 10 times every 5 s, arrow) of GCs induced robust LTP of SuM-GC oEPSCs. (*D*) The magnitude of depol-eLTP depends on the number of depolarizing pulses. Each protocol was applied to the different cells. Summary data at right shows the magnitude of LTP induced by different numbers of depolarizing pulses (once, 132 ± 13% of baseline, *n* = 11; three times, 167 ± 22% of baseline, *n* = 11; 10 times, 214 ± 11% of baseline, *n* = 11). One-way ANOVA, *P* < 0.001, Tukey's post hoc test **P* < 0.05; ****P* < 0.001. (*E*) Burst APs in GCs at θ frequency (10 bursts of 40-ms current injection, which elicited three to four APs, at 5 Hz, repeated five times every 5 s, arrow) induced LTP. (*Inset*) Example trace of a single burst APs. (*F*) Depol-eLTP was normally induced by repeated postsynaptic depolarizations (arrow) in the presence of 50 μM D-AP5. PPR was not changed after induction of depol-eLTP. (*Left*) Representative traces; (*Center*) time course summary plot of depol-eLTP (*Upper*) and normalized PPR (*Lower*); (*Right*) summary plot of PPR. Gray bars in (*B* and *C*) indicate the time windows for quantification of the magnitude of LTP. Here and in all figures, the magnitude of LTP was measured by comparing baseline responses with the last 10-min responses after LTP induction shown in each experiment. Data are presented as mean ± SEM.
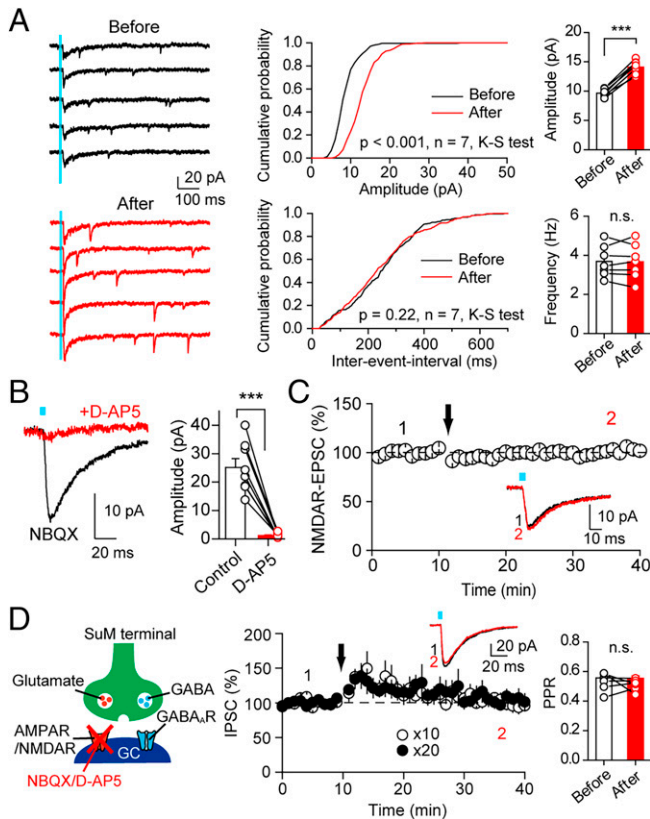
Fig. 2. Depol-eLTP at SuM-GC synapses is expressed postsynaptically, and GABAergic cotransmission is intact following GC depolarization. (*A*) The effect of postsynaptic depolarizations on asynchronous synaptic responses in the presence of Sr^{2+}. Representative traces (*Left*) of asynchronous SuM-GC oEPSCs before (10-min baseline) and after induction of depol-eLTP (20 min after GC depolarizations). (*Center*) Cumulative amplitude and inter-event interval distributions of asynchronous events obtained before and after depol-eLTP induction. (*Right*) Amplitude and frequency summary plots of asynchronous events obtained before and after depol-eLTP induction. For induction of depol-eLTP, extracellular Sr^{2+} solution was replaced by normal artificial cerebrospinal fluid (ACSF) containing Ca^{2+} after 10-min baseline. After confirming the induction of depol-eLTP, extracellular solution was returned to Sr^{2+}-containing ACSF. (*B*) SuM-GC NMDAR-oEPSCs were recorded at −60 mV in the presence of 10 µM NBQX and 100 µM picrotoxin (black trace). NMDAR-oEPSCs were completely blocked by 50 µM D-AP5 (red trace, $n = 8$, $P < 0.001$, paired t test). (*C*) The depol-eLTP induction protocol failed to induce LTP of NMDAR-oEPSCs. (*D*, *Left*) Schematic diagram illustrating blockade of glutamatergic transmission by NBQX and D-AP5 leaving GABAergic cotransmission intact at SuM-GC synapses. (*Center*) Repetitive postsynaptic depolarizations (open circles: 10 pulses; filled circles: 20 pulses) failed to induce LTP of SuM-GC oIPSCs. (*Right*) PPR of SuM-oIPSCs before and after (0 to 5 min after depolarization) 20 depolarizing pulses. Data are presented as mean ± SEM; ***$P < 0.001$. n.s., not significant.

AMPAR-oEPSCs, NMDAR-oEPSCs did not show LTP following postsynaptic depolarizations (Fig. 2*C*) (101 ± 4% of baseline, $n = 10$, $P = 0.85$, paired t test). These results also suggest that depol-eLTP is expressed postsynaptically.

In addition to excitatory synapses, several studies have demonstrated that postsynaptic depolarization induces LTP at inhibitory synapses in several brain regions (35–39). We examined the effects of postsynaptic depolarization on GABAergic cotransmission. Using an intracellular solution containing a high concentration of Cl^- (calculated $E_{Cl^-} = –20$ mV), we recorded optically evoked inhibitory postsynaptic currents (oIPSCs) from GCs as inward currents at –60 mV. Unlike AMPAR-oEPSCs, SuM-GC oIPSCs did not exhibit LTP by the depol-eLTP induction protocol (Fig. 2*D*) (105 ± 10% of baseline, $n = 12$, $P = 0.72$, Wilcoxon signed rank test), but showed transient potentiation (Fig. 2*D*) (0 to 5 min after

depolarization; 129 ± 47% of baseline, $n = 12$, $P < 0.01$, Wilcoxon signed rank test). Even stronger depolarizing pulses (20 times) elicited only transient potentiation (Fig. 2*D*) (0 to 5 min after depolarization; 132 ± 14% of baseline, $n = 6$, $P < 0.05$, paired t test), but not LTP of oIPSCs (Fig. 2*D*) (101 ± 8% of baseline, $n = 6$, $P = 0.87$, paired t test). As PPR was not changed during this transient potentiation (before: 0.56 ± 0.03; after: 0.55 ± 0.02, $n = 6$, $P = 0.52$, paired t test), postsynaptic change could be transiently induced after depolarization. Altogether, these results indicate that depolarization of GCs selectively induces a postsynaptic form of LTP of glutamatergic, but not GABAergic, cotransmission at SuM-GC synapses. Thus, selective expression of LTP at excitatory SuM-GC synapses increases the excitatory drive of glutamate/GABA corelease synapses.

Synapse Type and Target Cell-Specificity of Depol-eLTP. Given that postsynaptic depolarization causes neuron-wide Ca^{2+} influx, other inputs besides SuM may exhibit LTP by the depolarization of GCs. To test this possibility, the medial perforant-path (MPP), the main excitatory inputs from the entorhinal cortex (1), was extracellularly stimulated, and electrically evoked MPP-EPSCs and optically evoked SuM-oEPSCs were alternately recorded from the same GC (Fig. 3*A*). We found that the depol-eLTP induction protocol failed to induce LTP at MPP-GC synapses, while SuM-GC synapses exhibited LTP (Fig. 3*B*) (SuM: 198 ± 17% of baseline, $n = 11$, $P < 0.001$, paired t test; MPP: 112 ± 11% of baseline, $n = 11$, $P = 0.27$, paired t test). We also tested the effects of GC depolarization on inhibitory inputs originating from GABAergic INs. Pharmacologically isolated IPSCs were evoked using stimulation electrodes placed in the middle molecular layer or GC layer. In both inputs, postsynaptic depolarizations failed to induce LTP (*SI Appendix*, Fig. S3*A*). These results indicate that GC depolarization specifically induces depol-eLTP at glutamatergic SuM inputs to GCs.

We further examined whether depol-eLTP is SuM projection target cell-specific. We previously demonstrated that SuM neurons also make monosynaptic connections to GABAergic INs in the DG (14). To examine whether SuM-IN synapses undergo depol-eLTP, we recorded SuM-IN oEPSCs from INs in the DG (*SI Appendix, Supplementary Materials and Methods* and Fig. 3*C*). We found that the depol-eLTP induction protocol failed to induce LTP of SuM-IN oEPSCs, whereas SuM-GC oEPSCs exhibited LTP in interleaved slices (Fig. 3*D*) (IN: 94 ± 6% of baseline, $n = 10$, $P = 0.36$, paired t test; GC: 189 ± 29% of baseline, $n = 9$, $P < 0.01$, paired t test). The pairing protocol also failed to induce LTP at SuM-IN synapses (*SI Appendix*, Fig. S3*B*). In addition to the DG, the CA2 region is another main target of SuM afferents (5, 6, 40). We tested whether depolarization of CA2 pyramidal neurons could induce LTP at SuM-CA2 pyramidal neuron synapses. In agreement with recent reports (13, 41), light activation of the SuM fibers evoked oEPSCs recorded from CA2 pyramidal neurons (19.4 ± 3.4 pA, $n = 10$) (Fig. 3 *E* and *F*). In contrast to DG GCs, we found that depolarizations of CA2 pyramidal neurons did not trigger LTP at SuM-CA2 pyramidal neuron synapses (Fig. 3*F*) (100 ± 12% of baseline, $n = 10$, $P = 0.96$, paired t test). Taken together, these results indicate that SuM inputs express depol-eLTP in a target cell-specific manner, and GCs targeted by the SuM afferents exclusively exhibit depol-eLTP.

Depol-eLTP Requires Postsynaptic Ca^{2+} Increases, CaMKII, and SNARE-Dependent Exocytosis. Next, we investigated the postsynaptic mechanisms underlying depol-eLTP. As postsynaptic
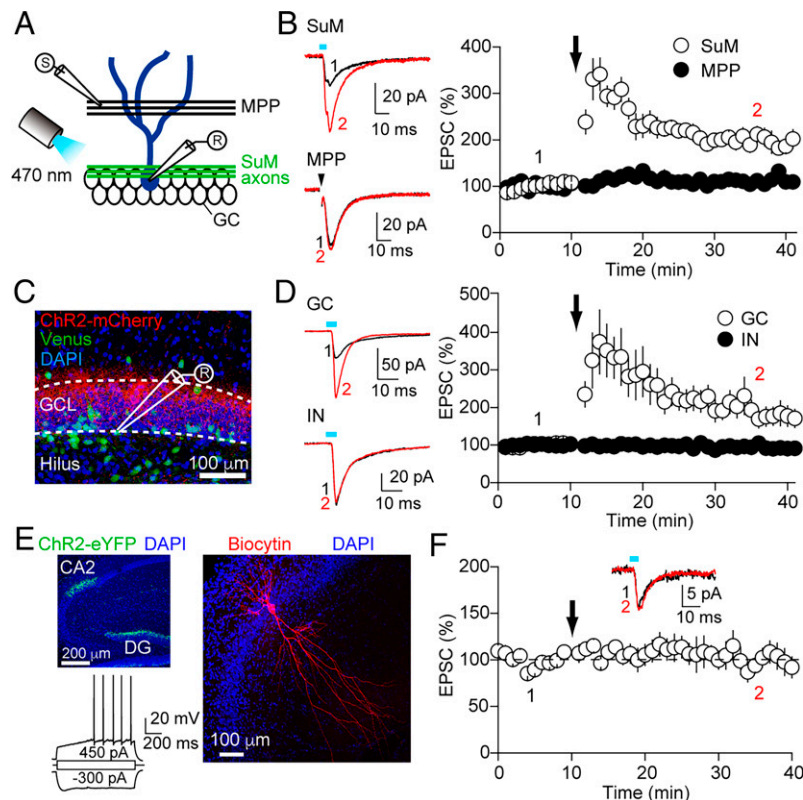
Fig. 3. SuM input-specificity and its target cell-specificity of depol-eLTP. (*A*) Schematic of recording of electrically evoked MPP-EPSCs and optically evoked SuM-EPSCs from the same GC. Each input was alternately stimulated every 10 s. (*B*) Repetitive depolarizing pulses of GCs (arrow) elicited LTP of SuM-oEPSCs but not MPP-EPSCs. (*C*) Experimental diagram. A confocal image of DG obtained from a VGluT2-Cre/VGAT-Venus mouse expressing ChR2(H134R)-mCherry in the SuM axons. Whole-cell recording was performed from a Venus⁺ IN. (*D*) Repetitive depolarizations of INs failed to induce LTP, while interleaved recordings from GCs exhibited depol-eLTP. (*E*, *Upper Left*) ChR2(H134R)-eYFP-expressing SuM axons project to CA2 in addition to the DG. (*Right*) A confocal image of a biocytin-filled CA2 pyramidal neuron. (*Lower Left*) Intrinsic electrophysiological properties in responses to 1-s current steps in a CA2 pyramidal neuron. As typical characteristics of CA2 pyramidal neurons, delayed APs and minimal sag were elicited by a positive and negative current injection, respectively. (*F*) The depol-eLTP induction protocol did not induce LTP at SuM-CA2 pyramidal neuron synapses. Data are presented as mean ± SEM.

depolarization triggers postsynaptic Ca^{2+} influx, we examined whether postsynaptic Ca^{2+} influx is necessary for the induction of depol-eLTP. Intracellular loading GCs with the Ca^{2+} chelator BAPTA (20 mM) completely abolished depol-eLTP (Fig. 4*A*) (104 ± 7% of baseline, $n = 11$, $P < 0.01$, compared with control, unpaired t test). Bath application of the L-VDCC blocker nifedipine (30 μM) also blocked depol-eLTP (Fig. 4*A*) (93 ± 10% of baseline, $n = 10$, $P < 0.001$, compared with control, Mann–Whitney U test). We excluded the involvement of Ca^{2+} release from internal stores in depol-eLTP, as pretreatment of slices with cyclopiazonic acid (CPA, 30 μM), a manipulation to deplete intracellular Ca^{2+} stores, did not block the induction of depol-eLTP (Fig. 4*B*) (227 ± 36% of baseline, $n = 5$, $P = 0.67$, compared with control, unpaired t test). These results indicate that depol-eLTP at SuM-GC synapses requires postsynaptic Ca^{2+} influx through L-VDCCs.

Several types of protein kinases, including protein kinase A (PKA), protein kinase C (PKC), and CaMKII, contribute to LTP induction (42–45). We examined whether the inhibitors of these kinases could block depol-eLTP. We found that neither the PKA inhibitor H89 (10 μM) nor the PKC inhibitor Gö6983 (1 μM) blocked the induction of depol-eLTP (Fig. 4 *C* and *D*) (H89: 186 ± 33% of baseline, $n = 8$, $P = 0.72$, compared with control, unpaired t test; Gö6983: 221 ± 16% of baseline, $n = 7$, $P = 0.91$, compared with control, unpaired t test). We confirmed that H89 and Gö6983 we used were effective, as mossy fiber LTP (46) and posttetanic potentiation in

the cerebellum (47) were blocked by H89 and Gö6983, respectively (*SI Appendix*, Fig. S4). Next, we examined the involvement of CaMKII in depol-eLTP. Bath application of the CaMKII inhibitor KN-93 (10 μM) abolished depol-eLTP (Fig. 4*E*) (114 ± 12% of baseline, $n = 6$, $P < 0.05$, compared with control, unpaired t test). To determine the potential contribution of postsynaptic CaMKII activity in depol-eLTP, we applied the specific CaMKII peptide inhibitor autocamtide-2–related inhibitory peptide (AIP, 10 μM) via a patch pipette. Loading GCs with AIP blocked depol-eLTP (Fig. 4*F*) (111 ± 13% of baseline, $n = 5$, $P < 0.05$, compared with control, unpaired t test). These results clearly indicate that depol-eLTP requires postsynaptic CaMKII activity.

We next investigated the postsynaptic expression mechanisms of depol-eLTP. Growing evidence indicates that the insertion of AMPARs via SNARE-dependent exocytosis in the postsynaptic plasma membrane is necessary for canonical NMDAR-dependent LTP at CA3-CA1 synapses (42, 43, 48). We tested whether similar mechanisms could mediate depol-eLTP. We found that postsynaptic loading with *N*-ethylmaleimide (NEM, 500 μM) and botulinum toxin-A (BoTx, 200 ng/mL), both of which inhibit SNARE-dependent exocytosis (49), abolished depol-eLTP (Fig. 4 *G* and *H*) (NEM: 102 ± 13% of baseline, $n = 7$, $P < 0.01$, compared with control, unpaired t test; BoTx: 87 ± 17% of baseline, $n = 7$, $P < 0.01$, compared with control, unpaired t test). These results suggest that depol-eLTP requires the exocytosis of AMPAR-containing vesicles.

Depolarization of GCs Induces NMDAR-Independent Unsilencing of SuM-GC Synapses. It is widely accepted that silent synapses, which contain NMDARs but no functional AMPARs, provide synaptic substrates for LTP in the young brain, and AMPAR unsilencing (insertion of AMPARs into the postsynaptic membrane) by correlated pre- and postsynaptic activity is implicated in postsynaptic mechanisms for NMDAR-dependent form of LTP (50). Because depol-eLTP is expressed postsynaptically and requires exocytosis of AMPARs, we sought to determine whether silent synapses could also exist at SuM-GC synapses, and postsynaptic depolarization could cause synapse unsilencing. By measuring the NMDAR/AMPAR ratio, we found that SuM-GC synapses showed higher NMDAR/AMPAR ratio than those of SuM-IN synapses (Fig. 5A). This observation implies that SuM-GC synapses may contain a large fraction of silent synapses (NMDAR-only synapses). Usually, for detecting silent synapses, no evoked AMPAR-EPSCs by sub-threshold fiber stimulation are recorded at negative membrane potentials, and then NMDAR-EPSCs are recorded at positive membrane potentials (50). However, under our experimental conditions, holding GCs at positive membrane potentials to record NMDAR-oEPSCs causes an influx of Ca^{2+}, which can induce LTP of AMPAR-oEPSCs at SuM-GC synapses.

To avoid this issue, we recorded both AMPAR- and NMDAR-oEPSCs at –60 mV, as recording of NMDAR-oEPSCs at –60 mV is feasible at SuM-GC synapses (Fig. 2B). In a subset of cells, when the intensity of light illumination was reduced, we observed oEPSCs, which showed a slow rise time (*Methods* and Fig. 5B). Following bath application of D-AP5, light illumination failed to evoke any responses, suggesting that baseline responses were mediated by NMDARs without AMPARs. Under these conditions, delivering the depol-eLTP induction protocol resulted in the long-lasting appearance of AMPAR-oEPSCs that were associated with a significant decrease in failure rate (Fig. 5 B and C) (before: 100%; LTP: $6.8 \pm 1.8\%$, $n = 9$, $P < 0.01$, Wilcoxon signed rank test) and an increase in efficacy (mean EPSC amplitude including failures) (Fig. 5C) (before: 1.7 ± 0.2 pA; LTP: 16.5 ± 1.0 pA, $n = 9$, $P < 0.001$, paired *t* test) and potency (mean EPSC amplitude excluding failures) (Fig. 5C) (before: 0 pA; LTP: 17.5 ± 1.0 pA, $n = 9$, $P < 0.01$, Wilcoxon signed rank test). In six of nine cells, we successfully recorded NMDAR-oEPSCs 30 min after washout of D-AP5 (sufficient time for full recovery of NMDAR-oEPSCs) ([SI Appendix](#), Fig. S5) and confirmed that the depol-eLTP induction protocol did not change the amplitude of NMDAR-oEPSCs (Fig. 5C) (before: 14.9 ± 1.6 pA; LTP: 14.3 ± 1.9 pA, $n = 6$, $P = 0.48$, paired *t* test). These results indicate that GC depolarization can cause NMDAR-independent synapse unsilencing through the incorporation of AMPARs into synapses.

MPP Inputs Heterosynaptically Trigger Depol-eLTP. Thus far, we have demonstrated that Ca^{2+} influx into GCs by their depolarization induces depol-eLTP. What is the input source for depolarizing GCs to trigger depol-eLTP under physiological conditions? Given that solo SuM inputs are too weak to excite GCs (14), other strong inputs, rather than SuM inputs, could effectively depolarize GCs and then heterosynaptically trigger depol-eLTP. Because the perforant path (PP) derived from the entorhinal cortex is the major input source to excite GCs (33, 51), we hypothesized that GC firing driven by PP inputs could trigger depol-eLTP. To address this possibility, we employed θ-burst stimulation (TBS), which is often used as an LTP-induction paradigm corresponding to the physiologically
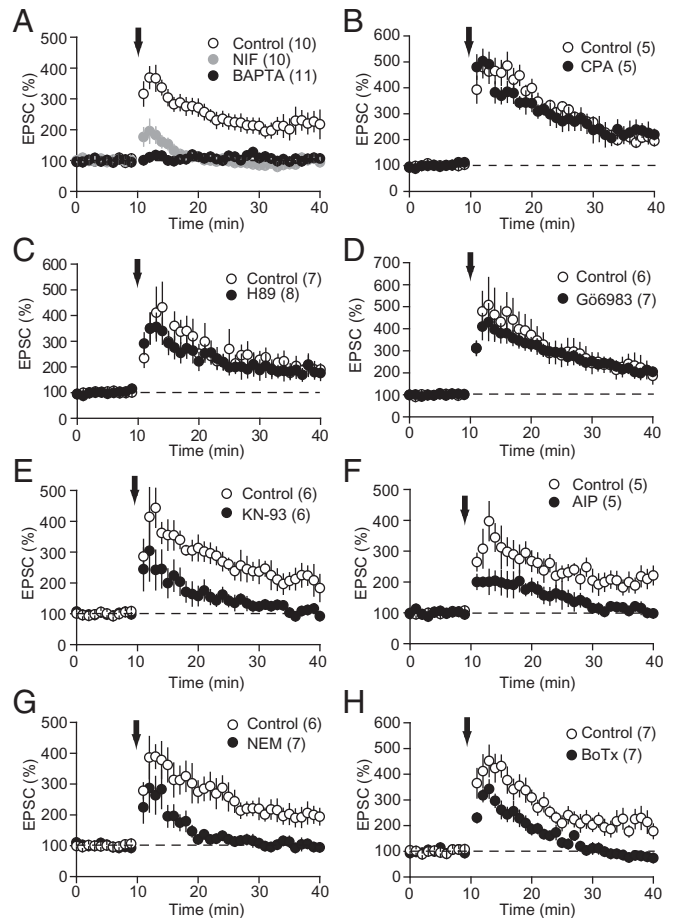

Fig. 4. Molecular mechanisms underlying depol-eLTP. (A) Depol-eLTP required a postsynaptic Ca^{2+} increase through L-VDCCs. Postsynaptic loading with 20 mM BAPTA failed to induce depol-eLTP. Postsynaptic depolarizations (arrow) abolished depol-eLTP in the presence of 30 μM nifedipine. Numbers in parentheses, here and in all figures, indicate the number of cells. (B) Depletion of intracellular Ca^{2+} stores by CPA (30 μM) had no effect on depol-eLTP. (C) Bath application of the PKA inhibitor H89 (10 μM) had no effect on depol-eLTP. (D) Bath application of the PKC inhibitor Gö6983 (1 μM) had no effect on depol-eLTP. (E) Bath application of the CaMKII inhibitor KN-93 (10 μM) abolished depol-eLTP. (F) Postsynaptic loading with the CaMKII inhibitor AIP (10 μM) abolished depol-eLTP. (G) Depol-eLTP was blocked by postsynaptic loading with NEM (500 μM). (H) Postsynaptic loading with BoTx (200 ng/mL) abolished depol-eLTP, while heat-inactivated BoTx (control) normally induced depol-eLTP. Data are presented as mean ± SEM.

relevant activity patterns of GCs (52–55), to evoke burst GC firing (Fig. 6A). After obtaining a 5-min baseline of SuM-GC oEPSCs in voltage-clamp mode, we switched to the current-clamp mode to allow the cell to generate APs and applied TBS to the MPP (Fig. 6B). The recording was then switched back into the voltage-clamp mode, and SuM-GC oEPSCs were monitored. We found that TBS of the MPP induced robust LTP at SuM-GC synapses (Fig. 6 B and C) ($196 \pm 16\%$ of baseline, $n = 6$, $P < 0.001$, paired *t* test). This LTP was completely blocked by postsynaptic application of BAPTA (Fig. 6C) ($101 \pm 10\%$ of baseline, $n = 5$, $P < 0.001$, compared with control, unpaired *t* test), suggesting that Ca^{2+} influx driven by TBS of the MPP is required for the induction of LTP. Similar to depol-eLTP, TBS-induced LTP was normally induced in the presence of D-AP5 ($198 \pm 24\%$ of baseline, $n = 8$, $P < 0.05$, Wilcoxon signed rank test) and blocked by 10 μM KN-93 ($117 \pm 11\%$ of baseline, $n = 5$, $P = 0.11$, paired *t* test) (Fig. 6D). Together, these results indicate that LTP at excitatory SuM-GC synapses can be heterosynaptically induced by MPP-mediated burst GC firing.

SuM Inputs Generate AP Firing in GCs after Induction of Depol-eLTP. Given that GC burst-firing selectively potentiates glutamatergic, but not GABAergic, cotransmission at SuM-GC synapses, depol-eLTP dramatically increases the excitatory drive of SuM inputs. Therefore, highly potentiated SuM glutamatergic inputs could generate AP firing in GCs even if SuM inputs cannot drive APs under basal conditions (14). To test this possibility, we monitored the SuM-induced APs in GCs before and after LTP induction. For this purpose, we performed gramicidin perforated-patch recordings to preserve the physiological intracellular Cl⁻ concentration. We confirmed that depol-eLTP was normally induced under gramicidin perforated-patch recordings (*SI Appendix*, Fig. S6A) and that E_{GABA} in GCs was -74.8 ± 2.3 mV ($n = 13$) (*SI Appendix*, Fig. S6B), which is similar to the previously reported E_{GABA} measured with gramicidin perforated-patch recordings from mature GCs (56–59). Previous studies have reported that the resting membrane potential of mature GCs is more negative than E_{GABA} (60–62). Accordingly, GABAergic action is depolarizing under resting conditions. To mimic this condition, we held the membrane potential between -80 and -85 mV (referred to as -80 mV) in the current-clamp mode with inhibition intact. Under these conditions, we found that brief-burst light illumination of SuM inputs (four pulses at 20 Hz) failed to induce APs in GCs (Fig. 7A). After a stable 5-min baseline, we delivered the depol-eLTP protocol under the voltage-clamp mode. Remarkably, the same burst stimulation triggered spike generation in 29% (7 of 24 cells) of GCs after LTP induction (Fig. 7A), suggesting that an increase in the excitatory drive of SuM inputs associated with depol-eLTP triggers GC firing.

We next examined how GABAergic cotransmission contributes to SuM input-evoked spike generation following LTP induction. Under blockade of inhibition by picrotoxin, in which brief-burst light illumination evoked no spikes, we found that LTP induction triggered a significant increase in spike generation (44%, 11 of 25 cells) compared with inhibition intact (Fig. 7 B, C, and E). These results suggest that GABAergic cotransmission negatively regulates glutamatergic SuM input-evoked GC firing. Given that glutamate and GABA are simultaneously released from the same SuM inputs, the inhibitory action of GABA is expected to be exerted via shunting inhibition (60, 63). In both conditions, most spikes were confined to the early time period (~10 min) after depol-eLTP induction, and there was no difference in the distribution of spike numbers (Fig. 7D). We further examined SuM input-evoked GC firing at a more depolarized membrane potential (between -60 to -65 mV, referred to as -60 mV) in which GABAergic action is hyperpolarizing. Similar to the more negative membrane potential (-80 mV), we found that burst stimulation evoked APs after LTP induction (36%, 9 of 25 cells) (Fig. 7F). When inhibition was blocked, the number of spikes and spike probability were increased (54%, 13 of 24 cells) (Fig. 7G, H, and J), and the spike generation lasted longer than control (Fig. 7I). Taken together, these results indicate that SuM inputs can drive GC output by induction of depol-eLTP, and GABAergic cotransmission contributes to the regulation of GC spike generation irrespective of the membrane potentials.

Discussion

In this study, we demonstrate that GC depolarization induces LTP of SuM-GC glutamatergic, but not GABAergic, cotransmission. This depol-eLTP requires postsynaptic Ca²⁺ elevation through L-VDCCs, postsynaptic CaMKII activity, and
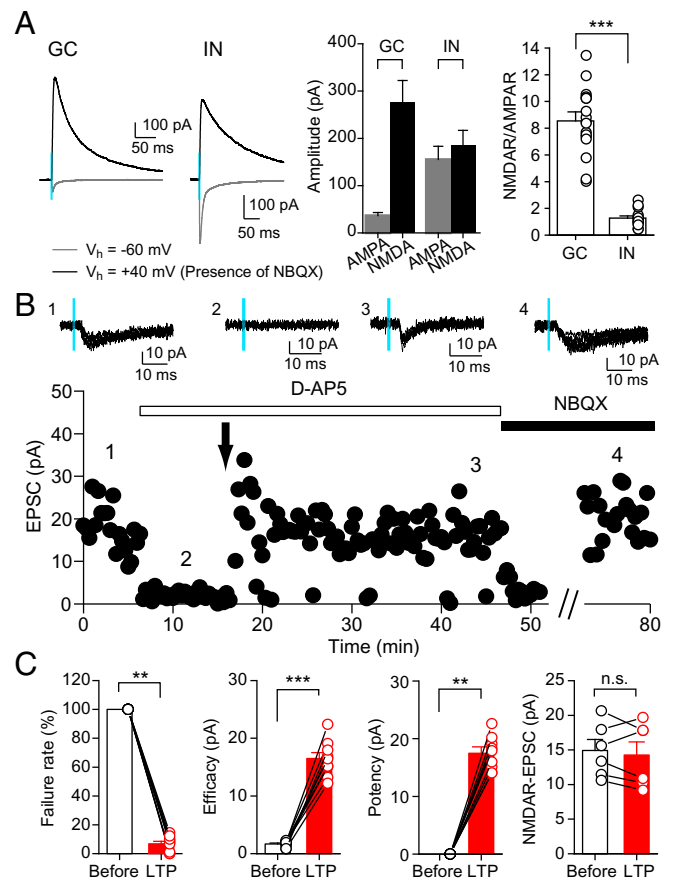

Fig. 5. High NMDAR/AMPAR ratio in GCs and synapse unsilencing induced by depolarization of GCs. (A) Marked difference in the NMDAR/AMPAR ratios at SuM-GC and SuM-IN synapses. (*Left*) oEPSCs recorded from GCs and INs at -60 mV and $+40$ mV. oEPSCs at $+40$ mV were recorded in the presence of 10 μM NBQX. (*Center*) Quantification of the amplitudes of AMPAR- and NMDAR-mediated currents recorded from GCs and INs. (*Right*) Summary data showing the NMDAR/AMPAR ratios (GC: 8.5 ± 0.67, $n = 17$; IN: 1.3 ± 0.16, $n = 15$, $P < 0.001$, unpaired t test). (B) Representative experiment of sample traces (*Upper*: six sweeps overlaid) and time course (*Lower*). oEPSCs evoked by weak light illumination at -60 mV showed slow rise time and were completely blocked by 50 μM D-AP5. Under this condition (no detectable oEPSCs), repetitive postsynaptic depolarizing pulses (arrow) elicited appearance of oEPSCs. NBQX (10 μM) was applied at the end of experiment to verify the response was mediated by AMPARs. After washout of D-AP5 in the presence of NBQX, NMDAR-oEPSCs were recovered without any potentiation. (C) Summary plots demonstrating that synapse unsilencing was associated with a significant decrease in failure rate, increase in efficacy and potency and no significant change in NMDAR-oEPSCs. Data are presented as mean ± SEM; **$P < 0.01$, ***$P < 0.001$. n.s., not significant.

exocytosis of AMPARs and is expressed postsynaptically. We further found that excitatory SuM-GC synapses included silent synapses, and the LTP induction protocol triggered synapse unsilencing, further supporting the postsynaptic origin of depol-eLTP. Remarkably, depol-eLTP is exclusively induced at SuM-GC synapses but not at MPP-GC, IN-GC, SuM-IN, or SuM-CA2 pyramidal neuron synapses. As a non-Hebbian form of plasticity, depol-eLTP was heterosynaptically induced by MPP-driven GC firing. We finally reveal that selective LTP of glutamatergic cotransmission at SuM-GC synapses makes excitatory effects dominate and consequently potentiates GC output. Our study clearly shows that the balance of glutamatergic/GABAergic cotransmission is rapidly modulated in an activity-dependent manner. Depol-eLTP at SuM-GC synapses may contribute to network activity in the DG and SuM-DG pathway-dependent neural functions.
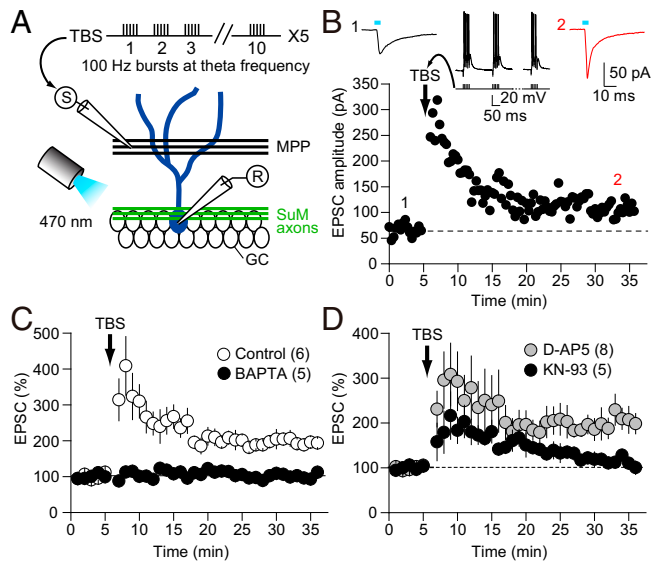
Fig. 6. TBS of MPP inputs heterosynaptically induces eLTP at SuM-GC synapses. (*A*) Schematic of recording configuration. MPP inputs were electrically stimulated by a glass electrode and ChR2-eYFP expressing SuM fibers were optically stimulated by a blue light pulse. For induction of LTP, MPP inputs were stimulated by TBS. (*B*) Representative experiment showing that TBS of MPP inputs (vertical arrow) induced robust LTP of SuM-GC oEPSCs. (*Inset*) APs during TBS. (*C*) Summary data showing that TBS-induced LTP was completely blocked by intracellular loading of BAPTA (20 mM). (*D*) TBS-induced LTP was induced in the presence of D-AP5 (50 µM) but blocked by bath application of KN93 (10 µM). Data are presented as mean ± SEM.

Activity-Dependent Change in the Balance of Glutamatergic and GABAergic Cotransmission at SuM-GC Synapses. Previous studies have reported that the balance of glutamate/GABA corelease in the lateral habenula was altered by depression and addiction (16, 19). In these neurological disorders, GABAergic cotransmission was reduced due to decreased expression of GAD or VGAT. In contrast to these chronic presynaptic alterations, depol-eLTP of SuM-GC synapses is rapidly expressed via postsynaptic modifications in response to physiological neural activity. Through this rapid alteration of glutamatergic/GABAergic cotransmission ratio, depol-eLTP can achieve dynamic modulation of GC activity.

To induce depol-eLTP, we delivered repetitive depolarizing pulses to GCs. To mimic more physiological situations, we further showed that GC burst firing or TBS of the MPP inputs can trigger LTP at excitatory SuM-GC synapses. It is known that GC activity in vivo is sparse (4). At first glance, this evidence may appear to make it unlikely that depol-eLTP is induced by the natural activity patterns of GCs. However, some GCs are more active and often fire in burst patterns (32–34, 64). Therefore, GC activity in behaving animals likely triggers Ca^{2+} increases strong enough to induce depol-eLTP. Particularly, "superburst" activity in GCs observed during mouse spatial navigation (34) may be suitable for the induction of depol-eLTP.

The balance between excitation and inhibition is essential for computation in the neuronal circuits, and feedback and feedforward inhibition generally control excitatory transmission (65). A unique property of glutamate/GABA corelease is that both neurotransmitters are released from the individual presynaptic terminals (18), achieving very local and rapid (without a monosynaptic delay mediated by feedforward inhibition) GABAergic inhibition. When the membrane potential of GCs was held at negative potential relative to E_{GABA}, blockade of GABAergic inhibition increased SuM input-evoked spike

probability, indicating that GABAergic cotransmission serves as inhibition despite the depolarizing action of GABA at resting potential. This shunting inhibition seems prominent in glutamate/GABA corelease synapses, as both neurotransmitters are synchronously released from the same terminals, providing spatially and temporally matched inhibition to excitatory cotransmission. This more targeted form of inhibition (66) than the typical disynaptic feedforward inhibition, which could be spatially isolated from excitatory inputs, may exclude the possibility that the action of GABAergic cotransmission of SuM inputs is depolarizing (60, 63). However, it should be noted that SuM neurons also excite dentate INs, driving feedforward inhibition to GCs (14, 15). Therefore, we cannot exclude the possibility that GABAergic inputs derived from feedforward inhibition recruited by SuM inputs contribute to regulation of GC firing.

We found that silent synapses exist at SuM-GC synapses, and the depol-eLTP induction protocol induced synapse unsilencing. In this study, we recorded from GCs with a low input resistance (< 300 MΩ), which are regarded as mature GCs (52). Given that silent synapses are generally observed in the young brain (50), our results suggest that mature GCs contain exceptionally abundant silent synapses at SuM-GC synapses. The sparse activity of GCs could account for our observations. If some GCs have never fired in bursts (silent GCs), such cells would not experience depol-eLTP, preventing NMDAR-only synapses from adding new AMPARs. It has been reported that dendritic complexity and the intrinsic excitability of GCs are correlated with GC activity (32, 64). Accordingly, silent GCs with less branched dendrites and low intrinsic excitability may account for a large fraction of NMDAR-only synapses at SuM-GC synapses. Future studies will have to investigate the relationship between dendritic morphology and proportion of silent synapses.

Mechanism of Depol-eLTP. Depol-eLTP is quite similar to the early studies showing that CA3-CA1 synapses elicit an L-VDCC–dependent, but NMDAR-independent form of LTP (28–30). A follow-up study demonstrated that an L-VDCC–dependent form of LTP induced by postsynaptic depolarization in the CA1 pyramidal neurons requires CaMKII and shares the same expression mechanisms with NMDAR-dependent LTP at CA3-CA1 synapses (31). NMDAR-dependent CA1 LTP is the most studied and best-known form of plasticity, thereby regarding this LTP as the primary model for understanding LTP. A widely accepted model of CA1 LTP (42, 43, 48, 67) indicates that two parallel pathways occur during the induction of LTP: trapping of surface diffusing AMPARs at the synapses and exocytosis of AMPAR-containing vesicles. Ca^{2+} entry through NMDARs initiates these processes, and once AMPARs move in the synapses, CaMKII and downstream signaling cascades contribute to the stabilization of receptors in the postsynaptic density (PSD). Given that depol-eLTP requires postsynaptic CaMKII activity and exocytosis of AMPARs, it seems likely that the postsynaptic Ca^{2+} increases through L-VDCCs rather than NMDARs trigger synaptic insertion of AMPARs via exocytosis of AMPARs and activation of CaMKII. The critical question is how L-VDCCs substitute for NMDARs. Generally, the localized Ca^{2+} elevation through NMDARs in the spine drives localized activation of CaMKII in the same spine to induce LTP (43).

Given that L-VDCCs trigger nonlocalized bulk Ca^{2+} increases, how does this Ca^{2+} increase activate CaMKII? Interestingly, SuM terminals make heterogeneous forms of synaptic contacts to GCs by forming symmetric and asymmetric
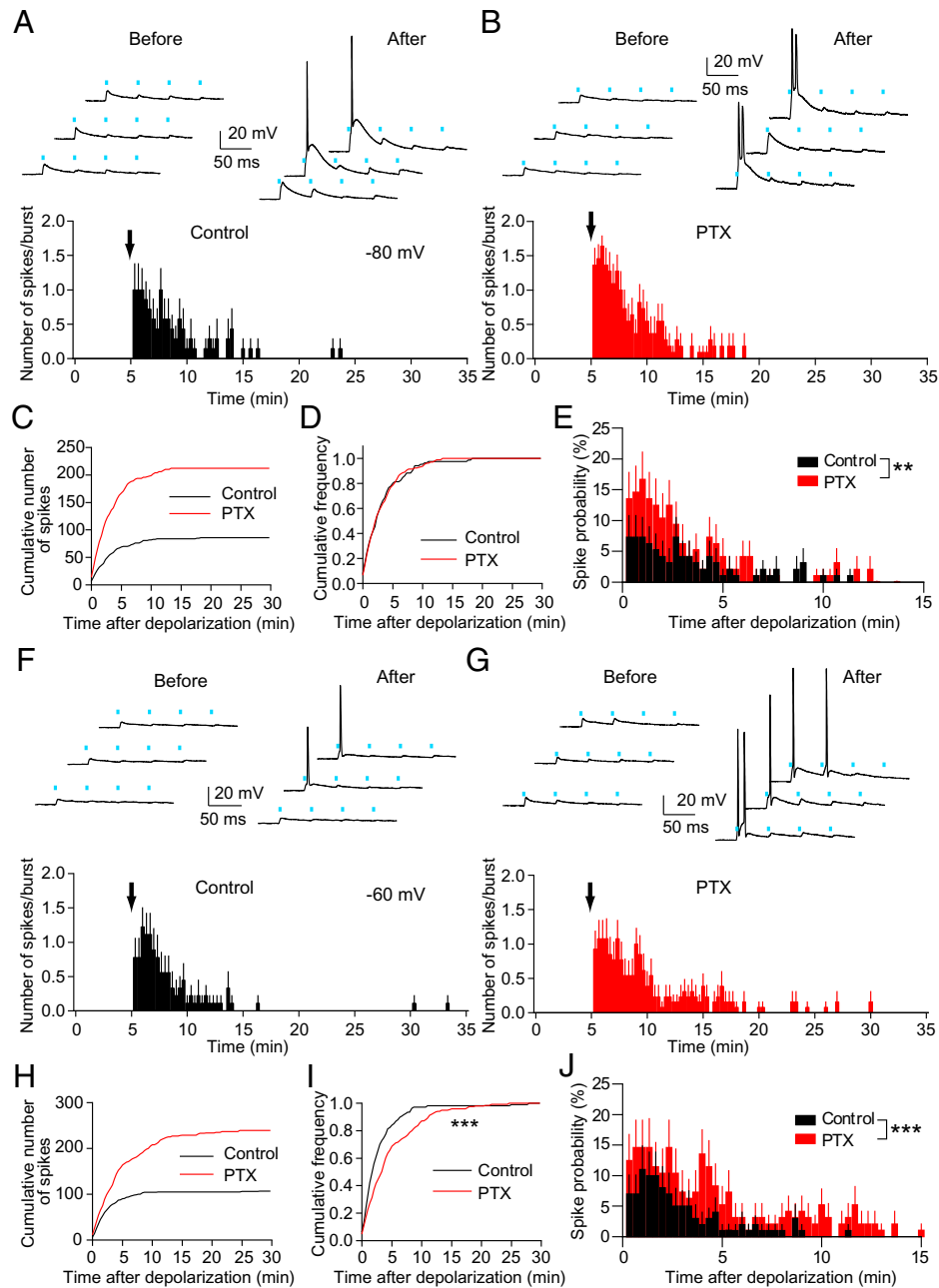
Fig. 7. SuM inputs trigger spike generation in GCs by increasing excitatory drive associated with the induction of depol-eLTP. (*A* and *B*, *Upper*) Representative traces showing GC firing elicited by burst light illumination (four pulses, 20 Hz) before and after induction of depol-eLTP in the control (*A*) and in the presence of 100 μM picrotoxin (PTX) (*B*). (*Lower*) Time-course plots of the number of spikes per burst (control, $n = 7$; PTX, $n = 11$). After 5-min baseline (no spike), the recording was switched to voltage-clamp mode, and GCs were depolarized repetitively to induce depol-eLTP (arrow). Membrane potential was held at −80 mV to −85 mV in current-clamp mode. (*C* and *D*) Cumulative number of spikes (*C*) and frequency (*D*) in control and PTX ($P = 0.054$, Kolmogorov–Smirnov test). (*E*) Time-course plot of the spike probability after induction of depol-eLTP in control ($n = 24$) and PTX ($n = 25$). In the presence of PTX, induction of depol-eLTP significantly increased spike probability ($P < 0.01$, two-way ANOVA). Nonspiking cells were included in the analysis. (*F* and *G*) Burst light illumination (four pulses, 20 Hz) was applied while GCs were held at −60 mV to −65 mV in current-clamp mode. Time-courses of the number of spikes per burst were plotted (control, $n = 9$; PTX, $n = 13$). (*H* and *I*) Cumulative number of spikes (*H*) and frequency (*I*) in control and PTX ($P < 0.001$, Kolmogorov–Smirnov test). (*J*) Time-course plot of the spike probability after induction of depol-eLTP in control ($n = 25$) and PTX ($n = 24$). In the presence of PTX, induction of depol-eLTP significantly increased spike probability ($P < 0.001$, two-way ANOVA). Nonspiking cells were included in the analysis. Data are presented as mean ± SEM; **$P < 0.01$, ***$P < 0.001$.

synapses on the soma, dendritic shafts, and spines (12, 68–70). Because increases in Ca^{2+} following depolarization are obviously different among the soma, dendritic shafts, and spines, it is likely that CaMKII activation is differently regulated by different Ca^{2+} levels in various subcellular compartments. For example, if L-VDCCs are localized close to the PSDs at the soma or dendritic shafts of SuM-GC glutamatergic synapses, local Ca^{2+} levels could be high enough to sufficiently activate

CaMKII to induce depo-eLTP. To reveal this, the distribution of L-VDCCs in SuM-GC synapses and the compartments of synapses that undergo depol-eLTP must be determined in future studies.

Depol-eLTP shows large transient potentiation immediately after postsynaptic depolarization, which was less affected by CaMKII inhibitors and inhibition of exocytosis. Similar results were found in NMDAR-dependent CA1 LTP, demonstrating

that inhibition of exocytosis does not affect early phase of LTP (49, 67, 71, 72). The early phase of potentiation is attributed to the capture of preexisting surface diffusing AMPARs (43, 67, 71, 73). Interestingly, we found that inhibition of glutamate uptake by DL-threo-β-benzyloxyaspartic acid (TBOA) increased SuM-GC oEPSCs, but not MPP-EPSCs (*SI Appendix,* *Fig. S7*). In general, inhibition of glutamate uptake influences the kinetics of AMPAR-EPSCs when AMPAR desensitization is blocked (74). Therefore, TBOA-induced increase in SuM-GC oEPSCs with AMPAR desensitization intact suggests that excitatory SuM-GC synapses may have exceptionally a large extrasynaptic pool of surface AMPARs (73). Further investigation will be required to examine whether these extrasynaptic AMPARs can contribute to the initiation of the early phase of potentiation by transient trapping in the PSD by Ca^{2+} influx. However, we cannot exclude the possibility that posttranslational modifications of AMPARs, such as increase in conductance and open probability, following depolarization-induced Ca^{2+} elevation may contribute to the early phase of potentiation.

Although somatic depolarization of GCs induces large Ca^{2+} elevation in both proximal and distal dendrites (75), depol-eLTP is observed exclusively at SuM inputs, but not at MPP inputs. Furthermore, SuM inputs elicit depol-eLTP specifically targeting GCs, but not INs and CA2 pyramidal neurons. What molecular mechanisms determine the synapse type- and target-specificity of LTP? There are several explanations for this. First, an unknown molecular sensor for Ca^{2+} ions may be specifically expressed in SuM-GC synapses and contribute to the increase in the number of synaptic AMPARs. Second, as prominent characteristics of excitatory SuM-GC synapses, we revealed a high NMDAR/AMPAR ratio and the existence of silent synapses. These findings imply that excitatory SuM-GC synapses may have many slots for trapping AMPARs (AMPAR-silent module) in the PSD (76). Finally, the location of synapses relative to the soma may be critical. Considering that backpropagating AP-induced Ca^{2+} transients show a distance-dependent attenuation in the GCs (77; but see ref. 75), a rise in the intracellular Ca^{2+} is higher in the SuM inputs at the soma or close to the soma, thereby reducing the threshold for the induction of depol-eLTP. Future studies should investigate all these possibilities.

Physiological Relevance of Depol-eLTP in the DG Network. We previously reported that SuM inputs have net excitatory effects on GCs and contribute to the facilitation of GC firing when associated with PP inputs (14). Our present study extends our previous results. Once depol-eLTP is induced, SuM inputs exert strong excitatory effects on GCs and elicit APs, especially within 10 min after LTP induction. After this period, SuM inputs failed to trigger spikes. This time window corresponds to the magnitude of oEPSC potentiation, showing huge potentiation followed by a stable potentiation phase. In the stable phase, potentiated SuM inputs associated with PP inputs can excite GCs more efficiently than under basal conditions. This suggests that depol-eLTP primes the SuM-GC synapses for GC firing. Thus, by establishing a new glutamatergic/GABAergic cotransmission ratio, solo SuM inputs or the

association of SuM and PP inputs can trigger enhancement of AP generation in GCs after LTP induction. A large population of SuM neurons is known to discharge rhythmically with a θ rhythm (78, 79). Therefore, if depol-eLTP is heterosynaptically induced by entorhinal cortical inputs, potentiated SuM inputs may frequently discharge GCs. The consequences of the GC output on its target are frequency dependent. High-frequency GC firing drives CA3 pyramidal neuron discharge, whereas low-frequency GC firing drives CA3 IN discharge (80). This GC firing frequency-dependent outcome in the CA3 pyramidal neurons implies that depol-eLTP might dramatically increase CA3 output through the enhancement of GC firing and consequently modulate the DG-CA3-CA1 trisynaptic circuit. Interestingly, a recent study reported that glutamatergic cotransmission at SuM-GC synapses is required for spatial memory retrieval (9). Given that memory engram GCs show LTP-like synaptic properties (81), depol-eLTP at SuM-GC synapses may be induced during memory formation, and after memory encoding and consolidation, depol-eLTP in engram GCs may contribute to memory retrieval through the potentiated SuM-DG excitatory pathway.

In addition to the SuM, GCs also receive local excitatory inputs from hilar mossy cells, which modulate GC activity through direct excitation and IN-mediated feedforward inhibition (82). It has been reported that presynaptic LTP is selectively expressed at mossy cell inputs onto GCs, but not at mossy cell inputs onto INs and facilitates GC output by increasing excitation/inhibition balance (83). Our study indicates that the DG network is dynamically regulated by mossy cell-mediated local and SuM-mediated subcortical pathways through two different forms of LTP.

Methods

Experiments were approved by the Animal Care and Use Committee of Doshisha University, and were performed in accordance with the guidelines of the committees. Whole-cell recordings were made from GCs, INs, and CA2 pyramidal neurons under an infrared differential interference contrast microscopy (Olympus, BX51WI). For voltage-clamp recordings, we used patch pipettes (3 to 6 MΩ) filled with an intracellular solution containing: 110 mM Cs-gluconate, 17.5 mM CsCl, 0.2 mM EGTA, 10 mM Hepes, 8 mM NaCl, 2 mM MgATP, 0.3 mM Na_3GTP, 10 mM phosphocreatine, pH 7.3 adjusted with CsOH (290 to 293 mOsm). For more details, see *SI Appendix, Supplementary Materials and Methods*.

Data Availability. All study data are included in the main text and *SI Appendix*.

1. D. G. Amaral, H. E. Scharfman, P. Lavenex, The dentate gyrus: Fundamental neuroanatomical organization (dentate gyrus for dummies). *Prog. Brain Res.* **163**, 3–22 (2007).
2. J. J. Knierim, J. P. Neunuebel, Tracking the flow of hippocampal computation: Pattern separation, pattern completion, and attractor dynamics. *Neurobiol. Learn. Mem.* **129**, 38–49 (2016).
3. T. D. Goode, K. Z. Tanaka, A. Sahay, T. J. McHugh, An integrated index: Engrams, place cells, and hippocampal memory. *Neuron* **107**, 805–820 (2020).
4. T. Hainmueller, M. Bartos, Dentate gyrus circuits for encoding, retrieval and discrimination of episodic memories. *Nat. Rev. Neurosci.* **21**, 153–168 (2020).
5. L. Haglund, L. W. Swanson, C. Köhler, The projection of the supramammillary nucleus to the hippocampal formation: An immunohistochemical and anterograde transport study with the lectin PHA-L in the rat. *J. Comp. Neurol.* **229**, 171–185 (1984).
6. R. P. Vertes, PHA-L analysis of projections from the supramammillary nucleus in the rat. *J. Comp. Neurol.* **326**, 595–622 (1992).

7. W. X. Pan, N. McNaughton, The supramammillary area: Its organization, functions and relationship to the hippocampus. *Prog. Neurobiol.* **74**, 127–166 (2004).

8. R. P. Vertes, B. Kocsis, Brainstem-diencephalo-septohippocampal systems controlling the theta rhythm of the hippocampus. *Neuroscience* **81**, 893–926 (1997).

9. Y. Li *et al.*, Supramammillary nucleus synchronizes with dentate gyrus to regulate spatial memory retrieval through glutamate release. *eLife* **9**, e53129 (2020).

10. N. P. Pedersen *et al.*, Supramammillary glutamate neurons are a key node of the arousal system. *Nat. Commun.* **8**, 1405 (2017).

11. L. Renouard *et al.*, The supramammillary nucleus and the claustrum activate the cortex during REM sleep. *Sci. Adv.* **1**, e1400177 (2015).

12. F. Billwiller *et al.*, GABA-glutamate supramammillary neurons control theta and gamma oscillations in the dentate gyrus during paradoxical (REM) sleep. *Brain Struct. Funct.* **225**, 2643–2668 (2020).

13. S. Chen *et al.*, A hypothalamic novelty signal modulates hippocampal memory. *Nature* **586**, 270–274 (2020).

14. Y. Hashimotodani, F. Karube, Y. Yanagawa, F. Fujiyama, M. Kano, Supramammillary nucleus afferents to the dentate gyrus co-release glutamate and GABA and potentiate granule cell output. *Cell Rep.* **25**, 2704–2715.e4 (2018).

15. M. I. Ajibola, J. W. Wu, W. I. Abdulmajeed, C. C. Lien, Hypothalamic glutamate/GABA cotransmission modulates hippocampal circuits and supports long-term potentiation. *J. Neurosci.* **41**, 8181–8196 (2021).

16. S. J. Shabel, C. D. Proulx, J. Piriz, R. Malinow, Mood regulation. GABA/glutamate co-release controls habenula output and is modified by antidepressant treatment. *Science* **345**, 1494–1498 (2014).

17. M. L. Wallace *et al.*, Genetically distinct parallel pathways in the entopeduncular nucleus for limbic and sensorimotor output of the basal ganglia. *Neuron* **94**, 138–152.e5 (2017).

18. D. H. Root *et al.*, Selective brain distribution and distinctive synaptic architecture of dual glutamatergic-GABAergic neurons. *Cell Rep.* **23**, 3465–3479 (2018).

19. F. J. Meye *et al.*, Shifted pallidal co-release of GABA and glutamate in habenula drives cocaine withdrawal and relapse. *Nat. Neurosci.* **19**, 1019–1024 (2016).

20. D. H. Root *et al.*, Single rodent mesohabenular axons release glutamate and GABA. *Nat. Neurosci.* **17**, 1543–1551 (2014).

21. J. H. Yoo *et al.*, Ventral tegmental area glutamate neurons co-release GABA and promote positive reinforcement. *Nat. Commun.* **7**, 13697 (2016).

22. K. A. Pelkey *et al.*, Paradoxical network excitation by glutamate release from VGluT3$^+$ GABAergic interneurons. *eLife* **9**, e51996 (2020).

23. C. Fasano *et al.*, Regulation of the hippocampal network by VGLUT3-positive CCK- GABAergic basket cells. *Front. Cell. Neurosci.* **11**, 140 (2017).

24. N. X. Tritsch, A. J. Granger, B. L. Sabatini, Mechanisms and functions of GABA co-release. *Nat. Rev. Neurosci.* **17**, 139–145 (2016).

25. N. Uchida, Bilingual neurons release glutamate and GABA. *Nat. Neurosci.* **17**, 1432–1434 (2014).

26. L. E. Trudeau, S. El Mestikawy, Glutamate cotransmission in cholinergic, gabaergic and monoamine systems: Contrasts and commonalities. *Front. Neural Circuits* **12**, 113 (2018).

27. R. C. Malenka, R. A. Nicoll, Long-term potentiation–A decade of progress? *Science* **285**, 1870–1874 (1999).

28. L. Aniksztejn, Y. Ben-Ari, Novel form of long-term potentiation produced by a K$^+$ channel blocker in the hippocampus. *Nature* **349**, 67–69 (1991).

29. L. M. Grover, T. J. Teyler, Two components of long-term potentiation induced by different patterns of afferent activation. *Nature* **347**, 477–479 (1990).

30. Y. Y. Huang, R. C. Malenka, Examination of TEA-induced synaptic enhancement in area CA1 of the hippocampus: The role of voltage-dependent Ca^{2+} channels in the induction of LTP. *J. Neurosci.* **13**, 568–576 (1993).

31. H. K. Kato, A. M. Watabe, T. Manabe, Non-Hebbian synaptic plasticity induced by repetitive postsynaptic action potentials. *J. Neurosci.* **29**, 11153–11160 (2009).

32. M. Diamantaki, M. Frey, P. Berens, P. Preston-Ferrer, A. Burgalossi, Sparse activity of identified dentate granule cells during spatial exploration. *eLife* **5**, e20252 (2016).

33. A. J. Pernía-Andrade, P. Jonas, Theta-gamma-modulated synaptic currents in hippocampal granule cells in vivo define a mechanism for network oscillations. *Neuron* **81**, 140–152 (2014).

34. D. Vandael, C. Borges-Merjane, X. Zhang, P. Jonas, Short-term plasticity at hippocampal mossy fiber synapses is induced by natural activity patterns and associated with vesicle pool engram formation. *Neuron* **107**, 509–521.e7 (2020).

35. O. Caillard, Y. Ben-Ari, J. L. Gaiarsa, Long-term potentiation of GABAergic synaptic transmission in neonatal rat hippocampus. *J. Physiol.* **518**, 109–119 (1999).

36. M. Kano, U. Rexhausen, J. Dreessen, A. Konnerth, Synaptic excitation produces a long-lasting rebound potentiation of inhibitory synaptic signals in cerebellar Purkinje cells. *Nature* **356**, 601–604 (1992).

37. T. Kurotani, K. Yamada, Y. Yoshimura, M. C. Crair, Y. Komatsu, State-dependent bidirectional modification of somatic inhibition in neocortical pyramidal cells. *Neuron* **57**, 905–916 (2008).

38. J. Lourenço *et al.*, Non-associative potentiation of perisomatic inhibition alters the temporal coding of neocortical layer 5 pyramidal neurons. *PLoS Biol.* **12**, e1001903 (2014).

39. A. R. Sieber, R. Min, T. Nevian, Non-Hebbian long-term potentiation of inhibitory synapses in the thalamus. *J. Neurosci.* **33**, 15675–15685 (2013).

40. K. Kohara *et al.*, Cell type-specific genetic and optogenetic tools reveal hippocampal CA2 circuits. *Nat. Neurosci.* **17**, 269–279 (2014).

41. V. Robert *et al.*, Local circuit allowing hypothalamic control of hippocampal area CA2 activity and consequences for CA1. *eLife* **10**, e63352 (2021).

42. B. E. Herring, R. A. Nicoll, Long-term potentiation: From CaMKII to AMPA receptor trafficking. *Annu. Rev. Physiol.* **78**, 351–365 (2016).

43. J. Lisman, R. Yasuda, S. Raghavachari, Mechanisms of CaMKII action in long-term potentiation. *Nat. Rev. Neurosci.* **13**, 169–182 (2012).

44. R. Malinow, H. Schulman, R. W. Tsien, Inhibition of postsynaptic PKC or CaMKII blocks induction but not expression of LTP. *Science* **245**, 862–866 (1989).

45. P. V. Nguyen, N. H. Woo, Regulation of hippocampal synaptic plasticity by cyclic AMP-dependent protein kinases. *Prog. Neurobiol.* **71**, 401–437 (2003).

46. M. G. Weisskopf, P. E. Castillo, R. A. Zalutsky, R. A. Nicoll, Mediation of hippocampal mossy fiber long-term potentiation by cyclic AMP. *Science* **265**, 1878–1882 (1994).

47. M. Beierlein, D. Fioravante, W. G. Regehr, Differential expression of posttetanic potentiation and retrograde signaling mediate target-dependent short-term synaptic plasticity. *Neuron* **54**, 949–959 (2007).

48. D. Choquet, Linking nanoscale dynamics of AMPA receptor organization to plasticity of excitatory synapses and learning. *J. Neurosci.* **38**, 9318–9329 (2018).

49. P. M. Lledo, X. Zhang, T. C. Südhof, R. C. Malenka, R. A. Nicoll, Postsynaptic membrane fusion and long-term potentiation. *Science* **279**, 399–403 (1998).

50. G. A. Kerchner, R. A. Nicoll, Silent synapses and the emergence of a postsynaptic mechanism for LTP. *Nat. Rev. Neurosci.* **9**, 813–825 (2008).

51. A. Bragin *et al.*, Gamma (40-100 Hz) oscillation in the hippocampus of the behaving rat. *J. Neurosci.* **15**, 47–60 (1995).

52. C. Schmidt-Hieber, P. Jonas, J. Bischofberger, Enhanced synaptic plasticity in newly generated granule cells of the adult hippocampus. *Nature* **429**, 184–187 (2004).

53. S. Ge, C. H. Yang, K. S. Hsu, G. L. Ming, H. Song, A critical period for enhanced synaptic plasticity in newly generated neurons of the adult brain. *Neuron* **54**, 559–566 (2007).

54. W. E. Skaggs, B. L. McNaughton, M. A. Wilson, C. A. Barnes, Theta phase precession in hippocampal neuronal populations and the compression of temporal sequences. *Hippocampus* **6**, 149–172 (1996).

55. C. Pavlides, Y. J. Greenstein, M. Grudman, J. Winson, Long-term potentiation in the dentate gyrus is induced preferentially on the positive phase of theta-rhythm. *Brain Res.* **439**, 383–387 (1988).

56. S. Heigele, S. Sultan, N. Toni, J. Bischofberger, Bidirectional GABAergic control of action potential firing in newborn hippocampal granule cells. *Nat. Neurosci.* **19**, 263–270 (2016).

57. J. H. Chancey *et al.*, GABA depolarization is required for experience-dependent synapse unsilencing in adult-born neurons. *J. Neurosci.* **33**, 6614–6622 (2013).

58. U. Kraushaar, P. Jonas, Efficacy and stability of quantal GABA release at a hippocampal interneuron-principal neuron synapse. *J. Neurosci.* **20**, 5594–5607 (2000).

59. C. Elgueta, M. Bartos, Dendritic inhibition differentially regulates excitability of dentate gyrus parvalbumin-expressing interneurons and granule cells. *Nat. Commun.* **10**, 5561 (2019).

60. P. H. Chiang *et al.*, GABA is depolarizing in hippocampal dentate granule cells of the adolescent and adult rats. *J. Neurosci.* **32**, 62–67 (2012).

61. J. F. Sauer, M. Strüber, M. Bartos, Interneurons provide circuit-specific depolarization and hyperpolarization. *J. Neurosci.* **32**, 4224–4229 (2012).

62. K. J. Staley, I. Mody, Shunting of excitatory input to dentate gyrus granule cells by a depolarizing GABAA receptor-mediated postsynaptic conductance. *J. Neurophysiol.* **68**, 197–212 (1992).

63. A. T. Gulledge, G. J. Stuart, Excitatory actions of GABA in the cortex. *Neuron* **37**, 299–309 (2003).

64. X. Zhang, A. Schlögl, P. Jonas, Selective routing of spatial information flow from input to output in hippocampal granule cells. *Neuron* **107**, 1212–1225.e7 (2020).

65. J. S. Isaacson, M. Scanziani, How inhibition shapes cortical activity. *Neuron* **72**, 231–243 (2011).

66. C. Q. Chiu *et al.*, Compartmentalization of GABAergic inhibition by dendritic spines. *Science* **340**, 759–762 (2013).

67. B. G. Hiester, M. I. Becker, A. B. Bowen, S. L. Schwartz, M. J. Kennedy, Mechanisms and role of dendritic membrane trafficking for long-term potentiation. *Front. Cell. Neurosci.* **12**, 391 (2018).

68. J. L. Boulland *et al.*, Vesicular glutamate and GABA transporters sort to distinct sets of vesicles in a population of presynaptic terminals. *Cereb. Cortex* **19**, 241–248 (2009).

69. J. A. Dent, N. J. Galvin, B. B. Stanfield, W. M. Cowan, The mode of termination of the hypothalamic projection to the dentate gyrus: An EM autoradiographic study. *Brain Res.* **258**, 1–10 (1983).

70. R. Soussi, N. Zhang, S. Tahtakran, C. R. Houser, M. Esclapez, Heterogeneity of the supramammillary-hippocampal pathways: Evidence for a unique GABAergic neurotransmitter phenotype and regional differences. *Eur. J. Neurosci.* **32**, 771–785 (2010).

71. A. C. Penn *et al.*, Hippocampal LTP and contextual learning require surface diffusion of AMPA receptors. *Nature* **549**, 384–388 (2017).

72. D. Wu *et al.*, Postsynaptic synaptotagmins mediate AMPA receptor exocytosis during LTP. *Nature* **544**, 316–321 (2017).

73. A. J. Granger, Y. Shi, W. Lu, M. Cerpas, R. A. Nicoll, LTP requires a reserve pool of glutamate receptors independent of subunit type. *Nature* **493**, 495–500 (2013).

74. A. V. Tzingounis, J. I. Wadiche, Glutamate transporters: Confining runaway excitation by shaping synaptic transmission. *Nat. Rev. Neurosci.* **8**, 935–947 (2007).

75. G. Stocca, C. Schmidt-Hieber, J. Bischofberger, Differential dendritic Ca^{2+} signalling in young and mature hippocampal granule cells. *J. Physiol.* **586**, 3795–3811 (2008).

76. J. Lisman, S. Raghavachari, A unified model of the presynaptic and postsynaptic changes during LTP at CA1 synapses. *Sci. STKE* **2006**, re11 (2006).

77. R. Krueppel, S. Remy, H. Beck, Dendritic integration in hippocampal dentate granule cells. *Neuron* **71**, 512–528 (2011).

78. I. J. Kirk, N. McNaughton, Supramammillary cell firing and hippocampal rhythmical slow activity. *Neuroreport* **2**, 723–725 (1991).

79. B. Kocsis, R. P. Vertes, Characterization of neurons of the supramammillary nucleus and mammillary body that discharge rhythmically with the hippocampal theta rhythm in the rat. *J. Neurosci.* **14**, 7040–7052 (1994).

80. D. A. Henze, L. Wittner, G. Buzsáki, Single granule cells reliably discharge targets in the hippocampal CA3 network in vivo. *Nat. Neurosci.* **5**, 790–795 (2002).

81. T. J. Ryan, D. S. Roy, M. Pignatelli, A. Arons, S. Tonegawa, Memory. Engram cells retain memory under retrograde amnesia. *Science* **348**, 1007–1013 (2015).

82. H. E. Scharfman, The enigmatic mossy cell of the dentate gyrus. *Nat. Rev. Neurosci.* **17**, 562–575 (2016).

83. Y. Hashimotodani *et al.*, LTP at hilar mossy cell-dentate granule cell synapses modulates dentate gyrus output by increasing excitation/inhibition balance. *Neuron* **95**, 928–943.e3 (2017).